CuCO₃–CuO nanocomposite as a novel and environmentally friendly catalyst for triazole synthesis†

Halima Hadj Mokhtar,[ab] Bouhadjar Boukoussa,*[cd] Rachida Hamacha,[c] Abdelkader Bengueddach[c] and Douniazad El Abed[a]

This paper focuses on the use of natural sources for the preparation of efficient and low cost catalysts. $CaCO_3$ is obtained from cuttlefish bone and was modified by the cation exchange of Ca^{2+} by Cu^{2+} in $CaCO_3$ using solutions of copper ($Cu(NO_3)_2$) at different concentrations. The modification of the solids was investigated using X-ray diffraction (XRD), Fourier transform infrared spectroscopy (FTIR), scanning electron microscopy (SEM), energy dispersive spectrometry (EDS) and ultraviolet-visible (UV-vis) spectroscopy. The results show that the copper exchanged materials contain a $CuCO_3$–CuO nanoparticle composite. The obtained solids were used as catalysts for the cycloaddition reaction of different azides with activated alkenes at room temperature under liquid phase conditions. The different parameters which affect the reaction were investigated such as reaction time, temperature of the reaction, effect of the copper content, catalyst mass, effect of the solvent and nature of the azide. High yields were obtained when the catalyst contained more copper. The best catalysts were calcined at different temperatures (200, 300, 400, 500 °C) in order to determine whether the active phase was $CuCO_3$ or CuO in the catalytic reaction. The XRD analysis of the calcined composites shows that an increase in calcination temperature leads to the formation of the CuO phase. On the other hand, the use of these calcined materials as catalysts shows that the active phase is copper carbonate. Finally, a new method for preparing triazoles with short reaction times was developed by the use of a cheap environmentally friendly catalyst.

1. Introduction

During the past few decades, the specific sizes, morphologies and crystallinities of inorganic materials have been considered as the factors responsible for their properties.[1–3] To date, scientists have focused on the synthesis of ordered structures with different morphologies and structures assembled by 1D and 2D nanostructures which are of great interest to chemists and materials scientists for their new properties and their fundamental importance in practical application areas.[4] Recently, a considerable effort has been devoted to investigating effective methods of synthesis of porous materials including

procedures in one step and those with a simple catalyst, which are highly desirable.[5]

$CaCO_3$ is the most abundant crystalline biomineral and has attracted the attention of researchers because of its different morphologies such as needle-shaped,[6] nano-spheres, rhombohedral-shaped,[7] lens-shaped, hexagonal-shaped,[8] and microspheres with urchin-shaped structures.[9] This material proved to be a suitable catalyst or catalyst support for different reactions such as the degradation of Acid Red B,[10] propylene epoxidation,[11] the oxidation of 1,2-dichlorobenzene,[5] biodiesel production,[12–14] homocoupling of aromatic halides,[15] the decomposition of acetylene,[16] the photo-catalysis of COD,[17] and the Fischer–Tropsch synthesis.[18]

Carbonate-based materials involve a large variety of cations such as Ca, Mg, Fe, Cu or Mn leading to different compositions, for example $CaCO_3$, $MgCO_3$, $CuCO_3$, $FeCO_3$, $MnCO_3$. The properties of these materials allow them to be used in a range of applications in food and pharmaceutical industries, and also as a filler in paper, and in plastic materials, catalysis, adsorption, medicine, electronics, ceramics, optics, pigments, cosmetics, and energy and magnetic applications.[18–25] The use of matrices containing copper in the catalysis field has received much attention over the past decades, due to the important basicity

[a]Laboratoire de Chimie Fine L.C.F, Université d'Oran 1 Ahmed Ben Bella, BP 1524 El M'naouer, 31100 Oran, Algeria

[b]Centre de Recherche Scientifique et Technique en Analyses Physico-Chimiques (C.R.A.P.C), BP 384, Bou-Ismail RP 42004 Tipaza, Algeria

[c]Laboratoire de Chimie des Matériaux L.C.M, Université d'Oran1 Ahmed Ben Bella, BP 1524 El-Mnaouer, 31000 Oran, Algeria. E-mail: bbouhdjer@yahoo.fr; Tel: +213 771663458

[d]Centre Universitaire Ain Témouchent, Institut des Sciences et de la Technologies, BP 284, 46000 Ain Témouchent, Algeria

† Electronic supplementary information (ESI) available. See DOI: 10.1039/c5ra17224a

and potential redox of copper,[26–28] the fact that the synthesis of a hybrid $CuCO_3$–CuO material is made much easier by using a copper precipitation method in the medium containing $CaCO_3$ or Na_2CO_3,[29–31] and the fact that the use of heating promotes the transformation of $CuCO_3$ to CuO. This gives a perspective on the use of these solids in different fields mainly in heterogeneous catalysis.

Previously, many publications were focused on the synthesis of triazoles. These organic products have been interesting in the development of novel compounds with anticonvulsant, antidepressant, antioxidant, anti-inflammatory, analgesic, antinociceptive, antibacterial, antimycobacterial, antifungal, antiviral, anticancer, anti-parasitic, anti-urease and other activities.[32–35] There are many methods for preparing triazole derivatives that have been developed,[36,37] and the use of a heterogeneous catalytic system has considerable synthetic advantages: wide availability of starting materials, short reaction times, simple reaction procedures, and an efficient catalyst for regeneration and separation.[38] Heterogeneous catalysts based on copper are greatly preferred for these types of reaction due to the presence of Cu^{2+}. In order to obtain the best catalytic performance for cycloaddition reactions, different catalysts based on copper are described in the literature such as: Cu/mesoporous materials,[39,40] copper nanoparticles (Cu NPs),[41] zeolite supported copper nanoparticles,[42] Cu/chitosan,[43] Cu/polymer catalysts[44] and others.

This work focuses on a facile and low cost synthetic method that leads to the direct transformation of $CaCO_3$ to $CuCO_3$–CuO nanostructured materials by the precipitation of $CaCO_3$ in a solution containing $Cu(NO_3)_2$. Furthermore, the cycloaddition reaction of different azides catalyzed by $CuCO_3$–CuO was also discussed based on experimental evidence. This contribution will also provide new insights into a better understanding of the reaction kinetics for the cycloaddition of azide-activated alkenes.

2. Experimental

2.1. Preparation procedure for catalysts

The material $CaCO_3$ was obtained from cuttlefish bone; it was recovered in the seashore areas in Ain el turck Oran Algeria, see Fig. 1. After grinding the solid and washing with ethanol to remove all organic traces, the recovered powder was treated with solutions containing different concentrations of $Cu(NO_3)_2$. After a few minutes stirring the product is formed as attested by the appearance of a blue precipitate. The obtained materials were filtered, washed and dried at 353 K. The concentrations of the copper nitrate solutions employed for the preparation of the catalysts are: 1 M, 0.8 M, 0.6 M, 0.4 M and 0.2 M, and the formed products are respectively named: MB1, MB0.8, MB0.6, MB0.4, MB0.2 and MB0 ($CaCO_3$ before treatment with copper solution).

2.2. Catalytic test

The catalytic reaction involves the preparation of a solution containing arylazides (1 mmol) in DMF (1 mL) (see Scheme 1), to which activated alkenes (1 mmol) and morpholine (1 mmol)
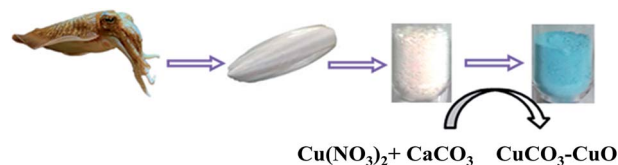

Fig. 1 Preparation of the nanocomposite $CuCO_3$–CuO using cuttlefish bone.

were firstly added, followed by the catalyst $CuCO_3$–CuO (20 mol%). The mixture was stirred for 1.5–4 h at room temperature. After the completion of the reaction, the precipitate formed upon the addition of H_2O (10 mL) and was filtrated, washed with H_2O and dried. To remove the catalyst, the precipitate was extracted with ethylacetate. After the removal of the solvent, the crude product was recrystallized (using EtOH).

2.3. Characterization

XRD powder diffraction patterns of $CaCO_3$ and the $CuCO_3$–CuO nanocomposite material were obtained with a Bruker D8 Advance X-ray diffractometer (40 kV, 30 mA) using CuKα radiation ($\lambda = 0.154$ nm) in the 2θ range of 5–70°. The surface topography of the different solids was observed using SEM on a Hitachi S-4800 microscope. An energy dispersive spectrometer (EDS), SAMx Diode: SiLi, marque: NORAN was used for the determination of the catalyst's chemical composition. FTIR spectra of the nanocomposite materials in the range of 400–4000 cm^{-1} were collected on a BRUKER ALPHA Platinum-ATR. Ultraviolet visible (UV-vis) absorbance spectra were recorded at room temperature on a Specord 210 Analytik Jena spectrometer.

3. Results and discussion

3.1. Catalyst characterization

The diffraction patterns of $CaCO_3$ and $CuCO_3$–CuO obtained at different concentrations of $Cu(NO_3)_2$ are given in Fig. 2. The XRD pattern of $CaCO_3$ obtained from cuttlefish bone is assigned to the aragonite structure. In fact, the diffraction peaks appearing in the ranges of $2\theta = 26.8$–27.6°, $2\theta = 33.3$–38.7°, $2\theta = 43.5$–46.4°, $2\theta = 49.1$–51° and $2\theta = 53.3$, are well matched with the standard pattern of the aragonite structure according to the literature.[45] For the case of the cuttlefish bone ($CaCO_3$) modified with different concentrations of $Cu(NO_3)_2$, we note that there was an appearance of two different phases. The first one's diffraction peaks appear at $2\theta = 12.9$°, $2\theta = 21.6$–24.7°, $2\theta = 32.4$–33.7°, $2\theta = 36.8$°, $2\theta = 40.1$°, $2\theta = 42.4$° and $2\theta = 44.1$° which correspond to a structure of copper carbonate $CuCO_3$, in agreement with the literature.[46] The second phase is related to the CuO structure and its diffraction peaks appear at $2\theta = 35.8$, $2\theta = 49.7$°, $2\theta = 52.2$ and $2\theta = 53.9$°. Once again these results are consistent with the literature.[46,47] The figure also shows that the peak intensities for CuO are much lower compared to those for the $CuCO_3$ phase.

The appearance of CuO can be explained by the drying temperature (80 °C) which as demonstrated by Teo *et al.*, plays a very important role in the decomposition of $CuCO_3$ into the
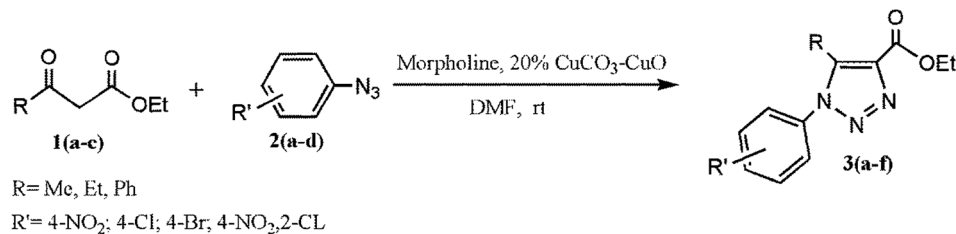
Scheme 1 Cycloaddition reaction of arylazides and activated alkenes using the nanocomposite $CuCO_3-CuO$ catalyst.
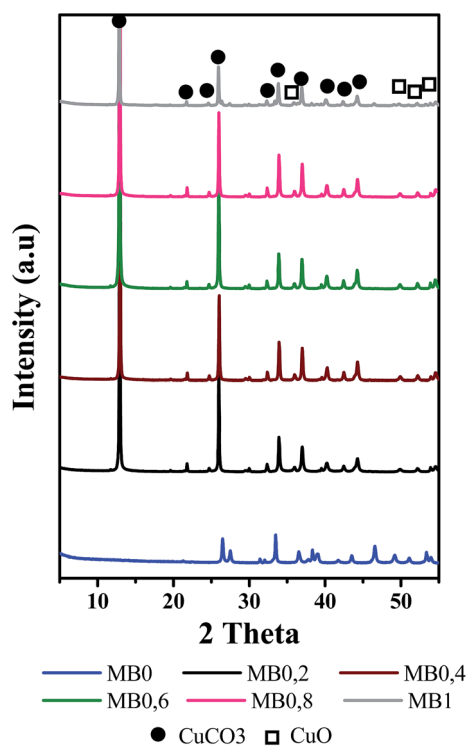

Fig. 2 XRD patterns of $CaCO_3$ and $CuCO_3-CuO$ with different Cu concentrations.
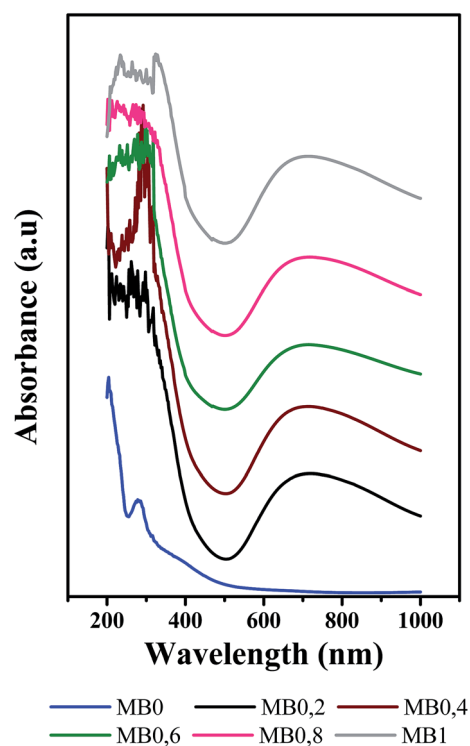

Fig. 3 UV-vis spectra of $CaCO_3$ and $CuCO_3-CuO$ with different Cu concentrations.

CuO structure, and when increasing the temperature, CuO formation is expected to be enhanced.[31] We also note that the concentration of copper affects the structure of the $CuCO_3-CuO$ material, and the highest peak intensity is obtained with moderate concentrations of $Cu(NO_3)_2$ (materials MB0.4 and MB0.6).

UV-vis reflectance diffuse spectra were recorded to investigate the coordination environment of the Cu species. Fig. 3 shows the UV-vis spectra of $CaCO_3$ and $CuCO_3-CuO$ with varying Cu content spanning from 200 nm to 1000 nm. All the materials exhibited intensive absorption centered around 282 nm for the case of $CaCO_3$ and 257–326 nm for $CuCO_3$, evidencing ligand-to-metal charge transfer between the oxygen ligand and the isolated Cu^{2+}.[48,49]

The intensity of this last band increased proportionally with the Cu loading, suggesting that more isolated Cu^{2+} ions were present in the composite $CuCO_3-CuO$. Furthermore a weak and broad absorption between 600 and 800 nm for all $CuCO_3$
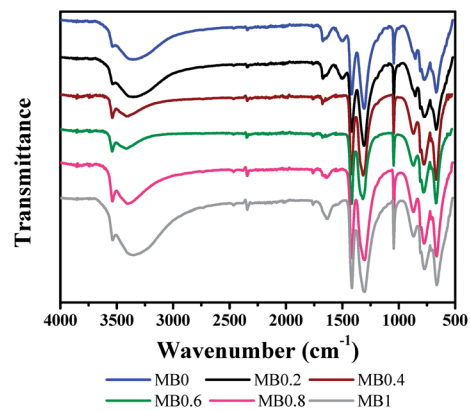

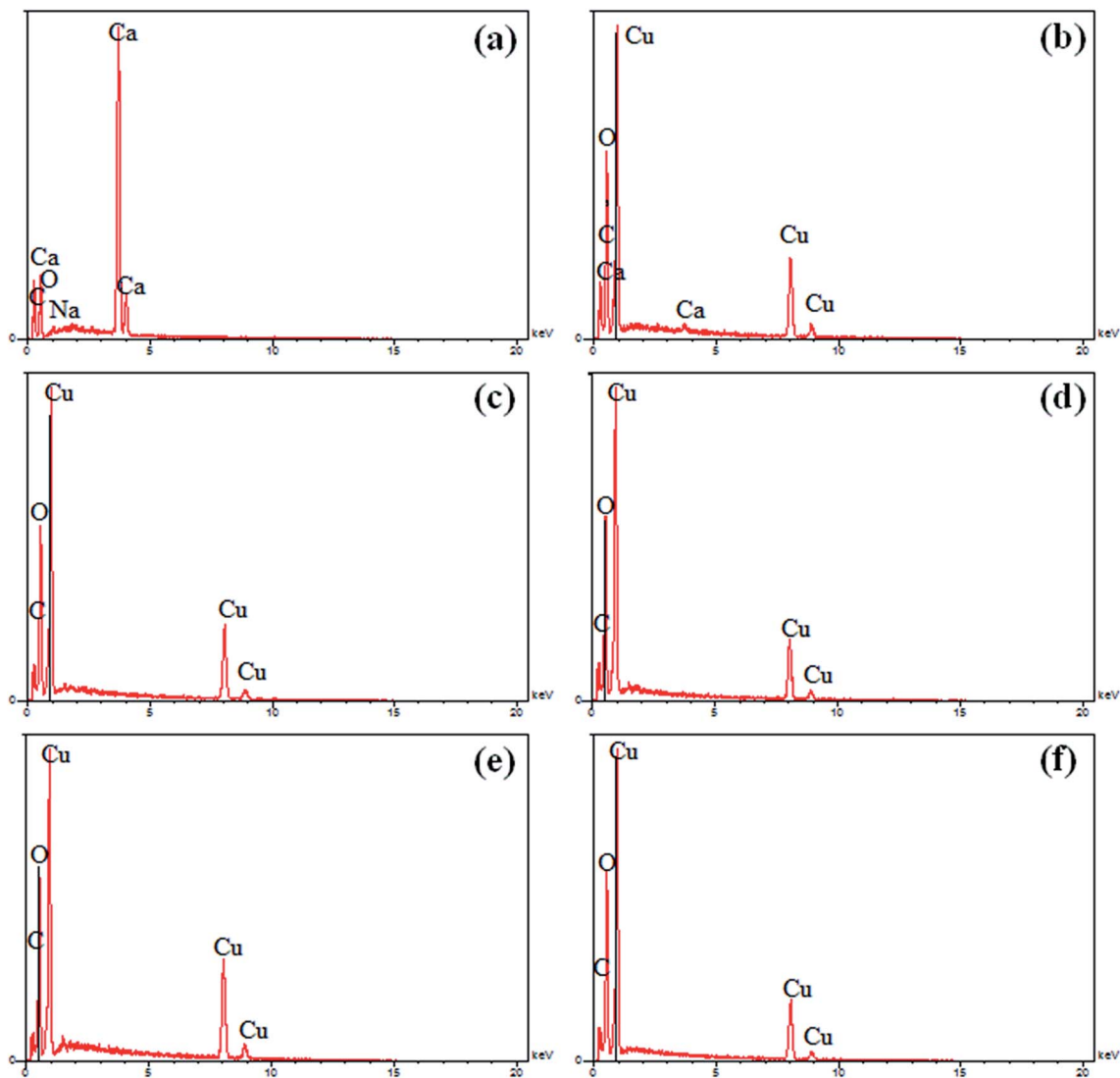Fig. 4 FT-IR spectra of $CaCO_3$ and $CuCO_3-CuO$ with different Cu concentrations.

Fig. 5 EDS of CaCO$_3$ and the composite CuCO$_3$–CuO with different copper concentrations; (a) MB0, (b) MB0.2, (c) MB0.4, (d) MB0.6, (e) MB0.8, (f) MB1.

materials was generally assigned to the formation of segregated CuO particles.[49,50] The much higher intensity of the peak between 230–300 nm, compared to that of the peak across the range of 600–800 nm, demonstrates that the isolated Cu^{2+} in the CuCO$_3$ phase are the predominant species in these materials. These results are consistent with the XRD data.

The FTIR data of the aragonite CaCO$_3$ and the CuCO$_3$–CuO composite obtained at different Cu(NO$_3$)$_2$ concentrations are given in Fig. 4. For the case of the aragonite CaCO$_3$ we can observe bands at 1673–1504 cm^{-1} (overtone and combination bands) attributed to the C=O groups of the carbonate ions.[51] The bands at 1423–1310 cm^{-1} (antisymmetric stretching mode), 1045 cm^{-1} (symmetric stretching mode), 852–806 cm^{-1} (out of plane bending mode) and 770–666 cm^{-1} (in plane bending mode) are attributed to the vibrations of the carbonate internal group C–O corresponding to the aragonite structure.[52] If the adsorption band of the O–H stretching vibration around 3542 cm^{-1} can be assigned to the presence of occluded water in the aragonite CaCO$_3$, the adsorption peak with a shoulder at 3335 cm^{-1} should be the O–H stretching vibration of crystal water and inter-particle hydrogen bonds.

The copper modified materials show some significant differences, indicating that physical and/or chemical changes occurred after copper adsorption. First, new peaks appear at 1538, 2342 and 2464 cm^{-1}, whereas the one peak at 1495 cm^{-1} disappears. Second, there is slight post-adsorption increase in the peak strength at 1538, 2342 cm^{-1} (Fig. 4). These IR spectra changes are most likely due to the ion-exchange between Cu^{2+} and Ca^{2+}. We also note that there was an increase in the band intensity between 3360–3542 (in the case of the MB1 sample) due to the water absorbed on the surface of the solids. On the other hand, there was a slight displacement of a few bands between 661 and 1636 cm^{-1}, due to the ion-exchange or electrostatic attraction on the surfaces during the exchange process.
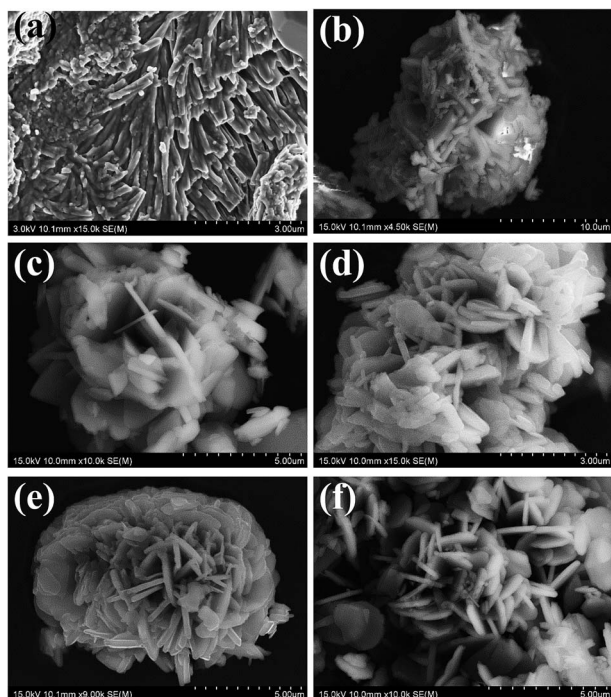
Fig. 6 SEM images of CaCO$_3$ and CuCO$_3$–CuO for different copper concentrations: (a) MB0, (b) MB0.2, (c) MB0.4, (d) MB0.6, (e) MB0.8, (f) MB1.
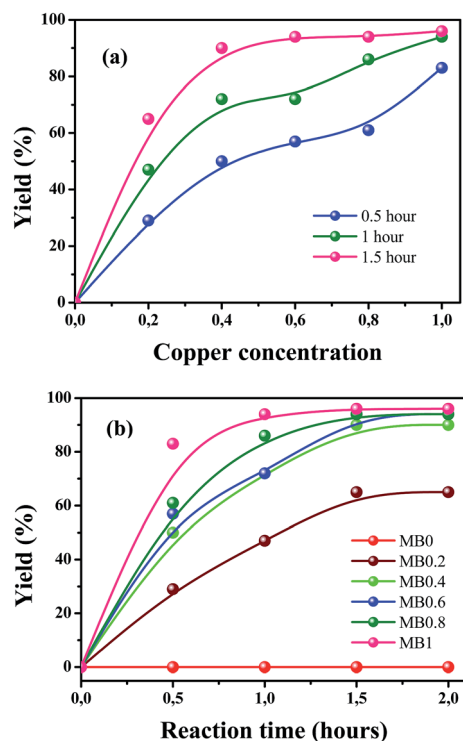

Fig. 7 Optimization of parameters for the cycloaddition reaction: (a) effect of copper concentration – 20 mol% of catalyst; (b) effect of reaction time.

The chemical composition of the solids was characterized using EDS measurements to confirm the presence of CaCO$_3$ and CuCO$_3$–CuO. The corresponding EDS spectra of the different samples are shown in Fig. 5. Fig. 5a presents the EDS spectrum of the MB0 sample which confirms the presence of CaCO$_3$ with no other impurities. Concerning the CaCO$_3$ modified by different concentrations of copper (MB0.4–MB1) in Fig. 5c–f, we note that the increase in the copper concentration causes an increased copper content in the solid structure (Fig. 5c–f). The tested concentrations generate the formation of a solid without any impurities, and the resulting solids consist essentially of C, Cu and O, except in the case of the solid MB0.2 which is formed by Ca, Cu, C and O. An obvious explanation for this is the formation of a solid which contains both CaCO$_3$ and CuCO$_3$–CuO with CuCO$_3$–CuO being the predominant species (Fig. 5b).
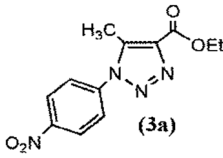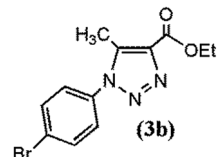
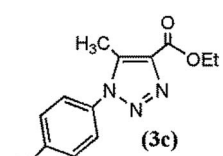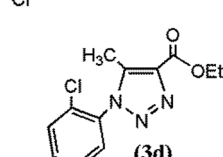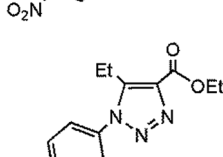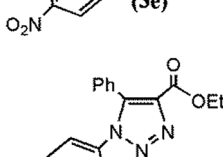Scanning electronic microscopy was used for the study of the morphology of the prepared materials. Fig. 6 shows SEM images of MB0 (pure CaCO$_3$) and the materials modified with different concentrations of copper, which were obtained following the precipitation method (see the experimental part). There is a major difference in the morphology of MB0 (pure CaCO$_3$) and MB0.2–MB1 (CuCO$_3$–CuO) as obtained by the precipitation method. Fig. 6a shows an image of cuttlefish bone (aragonite CaCO$_3$), and we can see that the nanostructure has a noodle-like morphology. Fig. 6c–f shows the SEM images of CuCO$_3$–CuO nanoplates where the thickness of the platelets is below 200 nm for MB0.6 (Fig. 6d) and the lateral dimensions are much bigger in comparison with the thickness (Fig. 6c–f). These results are very similar to the literature, and we also note that the changes in the morphologies depend on the increase in the copper concentration. As can be seen from Fig. 6d–f higher concentrations of copper generate spectacular morphologies in the case of MB1 (salad shaped) and MB0.8 (desert rose shaped). For the case of MB0.2 we observe that there is a mixture of aggregates that is due to the presence of several structures such as CaCO$_3$ and composite CuCO$_3$–CuO (Fig. 6b), these results were already confirmed by EDS analysis. The obtained information indicates that the copper concentration has a significant influence on the morphology and the connectivity of different nanoplates.

3.2. Catalytic experiments

Based on the results obtained in Fig. 7a and b we note that all the catalysts have a significant catalytic activity for the cycloaddition reaction except for the material CaCO$_3$.

The catalysts prepared at high concentrations of copper possess the best catalytic reactivity for the cycloaddition reaction (MB1 and MB0.8), and when using CuCO$_3$–CuO solids high yields of about 96% are obtained for a reaction time between 0.5 and 1.5 hours. Whereas, when using CaCO$_3$ no product has been obtained. This difference in activity is thus probably due to the presence of Cu^{2+} in the composite materials which has been obtained by cation exchange with Ca^{2+}. We note that not only do we reduce the reaction time, but also we have developed a simple process for the separation of the final product by filtration.

Table 1 Cycloaddition reaction of arylazide **1(a–c)** with activated alkenes **2(a–d)** performed at room temperature

Entry	R (**1**)	R′ (**2**)	Product (**3**)	Without CuCO$_3$–CuO[a]		With CuCO$_3$–CuO[b]	
				Yield[c] (%)	t (h)	Yield[c] (%)	t (h)
1	Me (**1a**)	4-NO$_2$ (**2a**)	(**3a**)	90	24	96	1.5
2	Me (**1a**)	4-Br (**2b**)	(**3b**)	64	24	40	2
3	Me (**1a**)	4-Cl (**2c**)	(**3c**)	61	24	60	4
4	Me (**1a**)	2-Cl,4-NO$_2$ (**2d**)	(**3d**)	90	24	90	1.5
5	Et (**1b**)	4-NO$_2$ (**2a**)	(**3e**)	80	24	79	1.5
6	Ph (**1c**)	4-NO$_2$ (**2a**)	(**3f**)	89	24	93	1.5

[a] Reaction conditions: arylazide **1(a–c)** (1 mmol), activated alkene **2(a–d)** (1 mmol), morpholine (1 mmol), DMF (1 mL), room temperature, 24 h. [b] Reaction conditions: arylazide **1(a–c)** (1 mmol), activated alkene **2(a–d)** (1 mmol), morpholine (1 mmol), CuCO$_3$–CuO (20 mol%), DMF (1 mL), room temperature, (1.5–4) h. [c] Isolated yields.

We also studied the effect of solvent on the cycloaddition reaction, and without the addition of morpholine, no product was obtained with the composite materials (see Table S1, ESI†) as catalysts which indicates that the presence of morpholine plays a very important role for activated alkenes. It is well known that nitrogen bases are used to accelerate triazole formation, in particular by coordinating to the catalytically active copper species, and promoting their liberation from the catalyst matrix, thus improving their thermodynamic stability.[53,54] Moreover, the basic character of the amines can contribute to the deprotonation of the alkyne and alkene components.[55,56]

If we compare our results with or without CuCO$_3$–CuO catalysts, the composite materials CuCO$_3$–CuO give the best catalytic performance for this reaction (see Table 1). The addition of active methylene, arylazides and DMF in the presence of morpholine without CuCO$_3$–CuO materials leads to the formation of triazoles with high yields after 24 hours of reaction time. The different heterocycle structures obtained were characterized using NMR spectroscopic analysis (NMR-H$^+$ and NMR-C^{13}) and Fourier transform infrared spectroscopy (FTIR) (see ESI†). In all cases with or without the catalyst composite we note that the halogen-substituted azides (Cl or Br) give moderate yields for the products (3b and 3c), because of the lower electro-attractor nature of Cl and Br compared to that of the nitro group.
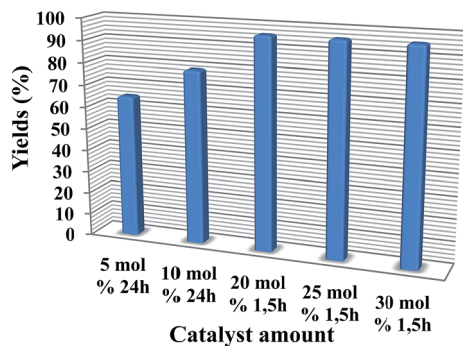
Fig. 8 Effect of the catalyst amount in the catalytic reaction: nitrophenylazides (1 mmol) in DMF (1 mL), ethyl aceto-acetate (1 mmol), morpholine (1 mmol) and $CuCO_3$–CuO (20 mol%).

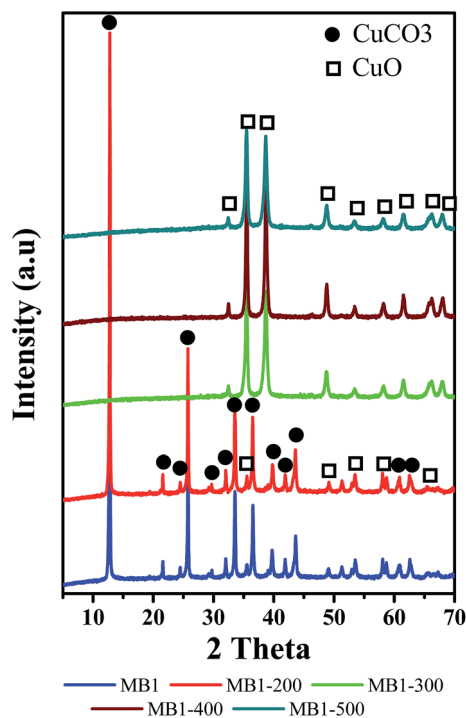**Fig. 10** FT-IR spectra of $CuCO_3$–CuO calcined at different temperatures.

Table 2 Effect of calcination temperature on the catalytic activity of the MB1 catalyst[c]

Catalysts	Temperature of calcination[a]	Phase	Yields
MB1	—	$CuCO_3$–CuO	96
MB1-200	200 °C	$CuCO_3$–CuO	54
MB1-300	300 °C	CuO	No product
MB1-400	400 °C	CuO	No product
MB1-500	500 °C	CuO	No product
CuO[b]	—	CuO	No product

[a] The catalysts were calcined for 2 hours. [b] CuO commercial SIGMA-ALDRICH. [c] Reaction conditions: arylazide **1(a)** (1 mmol), activated alkene **2(a)** (1 mmol), morpholine catalyst (20 mol%), DMF (1 mL), room temperature, 1.5 h.

Fig. 9 The XRD patterns of $CuCO_3$–CuO calcined at different temperatures.
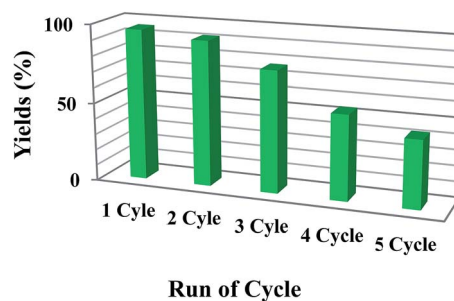
Fig. 11 Catalyst reusability. Reaction conditions 4-nitrophenyl azide (2 mmol), ethyl aceto-acetate (2 mmol), catalyst (20 mol%), DMF (2 mL), room temperature, reaction time: 1.5 h (15 min) (at the end of the reaction, the catalyst is dried and reused).

In order to understand the influence of the heterogeneous catalysts on the cycloaddition reaction, we have prepared a solution which contains nitrophenylazide (1 mmol) in DMF (1 mL), ethyl aceto-acetate (1 mmol) and morpholine (1 mmol) using different amounts of composite catalyst $CuCO_3$–CuO (MB1) (Fig. 8). Using 5 and 10 mol% of the composite material led to medium yields between 65 and 79% for a 24 h reaction time. However we can notice in Fig. 8 that increasing the amount of catalyst has a positive impact on the reaction yield, with an optimal value (96%) being obtained after 1.5 hours in the presence of 20–30% of catalyst.

In order to understand what is the catalytic active phase ($CuCO_3$ or CuO), we proposed to use the best catalyst MB1 at different temperatures of calcination (200, 300, 400 and 500 °C)
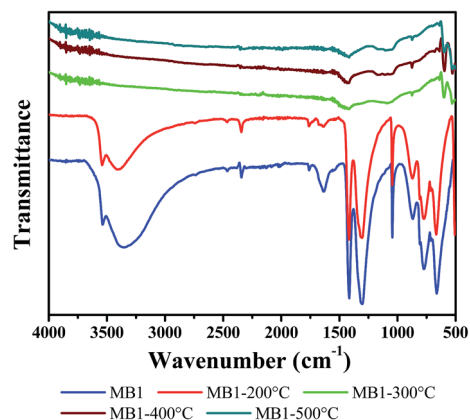
to get different forms of copper, and the obtained solids were characterized using XRD and FTIR as shown in Fig. 9 and 10.

The results obtained from XRD for the MB1 material treated at different temperatures of calcination shows that at 200 °C there is always the existence of two phases $CuCO_3$ and CuO, with the appearance of all the characteristic peaks of the $CuCO_3$ phase (Fig. 9), but beyond this value, we see the appearance of a single phase corresponding to CuO. These results are

consistent with the literature.[31] When can also deduce that a temperature of 300 °C is sufficient to transform all the copper carbonates to CuO.

Fig. 10 represents the FTIR spectra of $CuCO_3$–CuO treated at different temperatures. The FTIR analysis is in agreement with the XRD results. The material MB1 before and after calcination at 200 °C presents the same vibration (showing the existence of $CuCO_3$ and CuO), whereas for materials calcined between 300 and 500 °C, there has been a change in the vibration bands. We note the appearance of bands at 521 and 603 cm^{-1} which correspond to the stretching vibration of Cu–O bond in monoclinic CuO.[57] The vibration in the range of 600–1166 cm^{-1} (at 800 and 875 cm^{-1}) is attributed to the M–O stretching of CuO (M = Cu).[58] Further, a small and wide band at 1418 and 3271 cm^{-1} is ascribed to the vibrational modes of the O–H bond of the H_2O molecules physisorbed onto the surface of the CuO.[59]

The material MB1 obtained at different temperatures of calcination was used as a catalyst for the reaction of arylazide 1(a) with an activated alkene 2(a); the main results are listed in Table 2. From these results, we can conclude that the increase in the calcination temperature causes the formation of CuO particles. Their presence in the reaction medium has no effect on the reaction, thus the active phase in the reaction is copper carbonate $CuCO_3$.

The reusability of the catalysts has been studied in the cycloaddition of 4-nitrophenyl azide (1) under the following conditions: 4-nitrophenyl azide (2 mmol), ethyl aceto-acetate (2 mmol), $CuCO_3$–CuO (MB1, 20 mol%), DMF (2 mL), room temperature, 1.5 h reaction time. The catalysts were filtered, washed with DMF and dried before use in the following cycles, and the results are represented in Fig. 11. As it can be seen the catalyst could be reused up to three times with little loss of activity, the slight decrease in the yields may be due to the surface deactivation of the nanocomposite $CuCO_3$–CuO. We also note that the blue coloration of the catalyst before the reaction changed to a green color after 3 cycles of re-use due to the complexation of the catalysts with organic ligands in the reaction medium. These results were confirmed by XRD and FTIR analysis (see ESI Fig. S1 and S2†). From the fourth cycle there was a progressive decrease in the yields; in this stage we noticed that there was leaching of copper and the recovered catalyst lost its color due to the participation of copper in the reaction medium (see ESI Fig. S3†).

4. Conclusion

$CuCO_3$–CuO composite materials have been successfully prepared *via* a direct synthesis method using $Cu(NO_3)_2$ and cuttlefish bone. The method involves the use of a natural source for the preparation of efficient and low cost catalysts. The characterization methods show that the products formed by precipitation have a nanocomposite structure consisting of copper carbonate and copper oxide. The composites prepared at different copper concentrations show interesting results as catalysts for cycloaddition reactions and an increase in the copper content in the material leads to better results in the cycloaddition reaction, hence the MB1 nanocomposite material

gives the best yield achieved in a short reaction time (1 hour). We have confirmed that the increase of the calcination temperature causes the formation of CuO, and a calcination at about 300 °C is sufficient for the transformation of all $CuCO_3$ to the CuO phase. The use of MB1 at different temperatures of calcination allowed us to determine that the active phase is $CuCO_3$.

We showed that the reaction time, the nature of the azide used, and the catalyst mass play important roles in determining the yields of the product, and these catalysts may be used for three cycles. Beyond this value a decrease in yield has been obtained due to the leaching of copper into the reaction medium.

References

1 M. Olivares-Marín, E. M. Cuerda-Correa, A. Nieto-Sánchez, S. García, C. Pevida and S. Román, *Chem. Eng. J.*, 2013, **217**, 71–81.
2 G. Wang and W. Xu, *Polym. Degrad. Stab.*, 2013, **98**, 2323–2330.
3 K. de Witte, V. Meynen, M. Mertens, O. I. Lebedev, G. van Tendeloo, A. Sepúlveda-Escribano, F. Rodríguez-Reinoso, E. F. Vansant and P. Cool, *Appl. Catal., B*, 2008, **84**, 125–132.
4 Y.-X. Zhou, Q. Zhang, J.-Y. Gong and S.-H. Yu, *J. Phys. Chem. C*, 2008, **112**, 13383.
5 X. Ma, Q. Sun, X. Feng, X. He, J. Guo, H. Sun and H. Cao, *Appl. Catal., A*, 2013, **450**, 143–151.
6 M. Wang, H. K. Zou, L. Shao and J. F. Chen, *Powder Technol.*, 2004, **142**, 166–174.
7 D. Liu and M. Z. Yates, *Langmuir*, 2006, **22**, 5566.
8 N. Gehrke, H. Colfen, N. Pinna, M. Antonietti and N. Nassif, *Cryst. Growth Des.*, 2005, **5**, 1317.
9 W. Zhang, X. Li, Z. Qu, Q. Zhao and G. Chen, *Mater. Lett.*, 2010, **64**, 71–73.
10 X. Chen, C. Li, J. Wang, J. Li, X. Luan, Y. Li, R. Xu and B. Wang, *Mater. Lett.*, 2010, **64**, 1437–1440.
11 J. Lu, J. J. Bravo-Suárez, M. Haruta and S. T. Oyama, *Appl. Catal., A*, 2006, **302**, 283–295.
12 G. Galán Muciño, R. Romero, A. Ramírez, S. Luz Martínez, R. Baeza-Jiménez and R. Natividad, *Fuel*, 2014, 138143–138148.
13 L.-S. Hsieh, U. Kumar and J. C. S. Wu, *Chem. Eng. J.*, 2010, **158**, 250–256.
14 W. Wei Sheng Ho, H. Kiat Ng and S. Gan, *Bioresour. Technol.*, 2012, **125**, 158–164.
15 M. Zeng, Y. Du, C. Qi, S. Zuo, X. Li, L. Shao and X.-M. Zhang, *Green Chem.*, 2011, **13**, 350.
16 C.-T. Hsieh, Y.-T. Lin, J.-Y. Lin and J.-L. Wei, *Mater. Chem. Phys.*, 2009, **114**, 702–708.
17 B. Gao, L. Liu, J. Liu and F. Yang, *Appl. Catal., B*, 2013, **138–139**, 62–69.
18 M. A. M. Motchelaho, H. Xiong, M. Moyo, L. L. Jewell and N. J. Coville, *J. Mol. Catal. A: Chem.*, 2011, **335**, 189–198.
19 S.-L. Fu, Q. Song and Q. Yao, *Chem. Eng. J.*, 2015, **262**, 9–17.
20 C. Wang, C. He, Z. Tong, X. Liu, B. Ren and F. Zeng, *Int. J. Pharm.*, 2006, **308**, 160–167.

21 C. Qin, B. Feng, J. Yin, J. Ran, L. Zhang and V. Manovic, *Chem. Eng. J.*, 2015, **262**, 665–675.

22 I. Takahara, K. Murata, K. Sato, Y. Miura, M. Inaba and Y. Liu, *Appl. Catal., A*, 2013, **450**, 80–87.

23 B. Yao, Z. Ding, X. Feng, L. Yin, Q. Shen, Y. Shi and J. Zhang, *Electrochim. Acta*, 2014, **148**, 283–290.

24 K. Zhang, S. Wu, X. Wang, J. He, B. Sun, Y. Jia, T. Luo, F. Meng, Z. Jin, D. Lin, W. Shen, L. Kong and J. Liu, *J. Colloid Interface Sci.*, 2015, **446**, 194–202.

25 F. M. Hossain, B. Z. Dlugogorski, E. M. Kennedy, I. V. Belova and G. E. Murch, *Solid State Commun.*, 2010, **150**, 848–851.

26 G. Stavbera and Z. Časar, *Appl. Organomet. Chem.*, 2013, **27**, 159–165.

27 M. Casielloa, A. Monopoli, P. Cotugno, A. Milella, M. Michela Dell'Anna, F. Ciminale and A. Nacci, *J. Mol. Catal. A: Chem.*, 2014, **381**, 99–106.

28 F. Yu, F. Li, B. Zhang, H. Li and L. Sun, *ACS Catal.*, 2015, **5**, 627–630.

29 M. H. Habibi and B. Karimi, *J. Ind. Eng. Chem.*, 2014, **20**, 925–929.

30 J.-M. Sun, X.-H. Zhao and J.-C. Huang, *Chemosphere*, 2005, **58**, 1003–1010.

31 C.-H. Teo, Y. Zhu, X. Gao, A. T.-S. Wee and C.-H. Sow, *Solid State Commun.*, 2008, **145**, 241–245.

32 S. Güniz Küçükgüzel and P. Çıkla-Süzgün, *Eur. J. Med. Chem.*, 2015, **97**, 830–870.

33 K. Tamura, K. Inoue, M. Takahashi, S. Matsuo, K. Irie, Y. Kodama, T. Gamo, S. Ozawa and M. Yoshida, *Food Chem. Toxicol.*, 2015, **78**, 86–95.

34 J. Flieger, M. Tatarczak-Michalewska, M. Wujec, M. Pitucha and R. Świeboda, *J. Pharm. Biomed. Anal.*, 2015, **107**, 501–511.

35 S. Mahdieh Hashemi, H. Badali, H. Irannejad, M. Shokrzadeh and S. Emami, *Bioorg. Med. Chem.*, 2015, **23**, 1481–1491.

36 R. Huisgen, *Angew. Chem.*, 1963, **75**, 604–637.

37 V. V. Rostovtsev, L. G. Green, V. V. Fokin and K. B. Sharpless, *Angew. Chem., Int. Ed.*, 2002, **41**, 2596–2599.

38 B. Boukoussa, S. Zeghada, G. Bentabed Ababsa, R. Hamacha, A. Derdour, A. Bengueddach and F. Mongin, *Appl. Catal., A*, 2015, **489**, 131–139.

39 S. Roy, T. Chatterjee, M. Pramanik, A. S. Ro, A. Bhaumik and S. Manirul Islam, *J. Mol. Catal. A: Chem.*, 2014, **386**, 78–85.

40 I. Jlalia, F. Gallier, N. Brodie-Linder, J. Uziel, J. Augé and N. Lubin-Germain, *J. Mol. Catal. A: Chem.*, 2014, **393**, 56–61.

41 M. Nasrollahzadeh and S. Mohammad Sajadi, *J. Colloid Interface Sci.*, 2015, **457**, 141–147.

42 M. Nasrollahzadeh, S. Mohammad Sajadi, A. Rostami-Vartooni and M. Khalaj, *J. Colloid Interface Sci.*, 2015, **453**, 237–243.

43 K. Martina, S. E. S. Leonhardt, B. Ondruschka, M. Carini, A. Binello and G. Cravotto, *J. Mol. Catal. A: Chem.*, 2011, **334**, 60–64.

44 T. R. Chan and V. V. Fokin, *QSAR Comb. Sci.*, 2007, **26**, 1274–1279.

45 A. Ben Nasr, K. Walha, C. Charcosset and R. Ben Amar, *J. Fluorine Chem.*, 2011, **132**, 57–62.

46 W. N. R. Wan Isahak, Z. A. Che Ramli, M. Wafiuddin Ismail, K. Ismail, R. M. Yusop, M. W. Mohamed Hisham and M. Ambar Yarmo, *J. CO$_2$ Util.*, 2013, **2**, 8–15.

47 J.-H. Kim, A. Katoch, S.-W. Choi and S. Sub Kim, *Sens. Actuators, B*, 2015, **212**, 190–195.

48 H. T. Gomes, P. Selvam, S. E. Dapurkar, J. L. Figueiredo and J. L. Faria, *Microporous Mesoporous Mater.*, 2005, **86**, 287–294.

49 S. Velu, L. Wang, M. Okazaki, K. Suzuki and S. Tomura, *Microporous Mesoporous Mater.*, 2002, **54**, 113–126.

50 S. Sonia, I. Jose Annsi, P. Suresh Kumar, D. Mangalaraj, C. Viswanathan and N. Ponpandian, *Mater. Lett.*, 2015, **144**, 127–130.

51 S.-W. Lee, Y.-N. Jang, K.-W. Ryu, S.-C. Chae, Y.-H. Lee and C.-W. Jeon, *Micron*, 2011, **42**, 60–70.

52 F. Z. Zakaria, J. Mihaly, I. Sajo, R. Katona, L. Hajba, F. A. Aziz and J. Mink, *J. Raman Spectrosc.*, 2008, **39**, 1204–1209.

53 M. Meldal and C. W. Tornøe, *Chem. Rev.*, 2008, **108**, 2952–3015.

54 R. Berg and B. F. Straub, *Beilstein J. Org. Chem.*, 2013, **9**, 2715–2750.

55 G.-C. Kuang, P. M. Guha, W. S. Brotherton, J. T. Simmons, L. A. Stankee, B. T. Nguyen, R. J. Clark and L. Zhu, *J. Am. Chem. Soc.*, 2011, **133**, 13984–14001.

56 S. Zeghada, G. Bentabed-Ababsa, A. Derdour, S. Abdelmounim, L. R. Domingo, J. A. Saez, T. Roisnel, E. Nassar and F. Mongin, *Org. Biomol. Chem.*, 2011, **9**, 4295–4305.

57 V. V. T. Padil and M. Cernik, *Int. J. Nanomed.*, 2013, **8**, 889–898.

58 Y. Xu, D. Chen, X. Jiao and K. Xue, *Mater. Res. Bull.*, 2007, **42**, 1723–1731.

59 A. N. Ejhieh and H. Z. Mobarakeh, *J. Ind. Eng. Chem.*, 2014, **20**, 1421–1431.